Environmental Science and Pollution Research (2019) 26:32345–32359
https://doi.org/10.1007/s11356-019-06516-w

RESEARCH ARTICLE

Preparation of polyglycerol mediated superparamagnetic graphene oxide nanocomposite and evaluation of its adsorption properties on tetracycline

Binglong Yu[1] · Jie Wang[1] · Xiaoxin Yang[1] · Wenlong Wang[1] · Xiulan Cai[1]

Received: 21 July 2019 / Accepted: 10 September 2019 / Published online: 11 October 2019

Abstract

In this paper, we synthesized a polyglycerol(PG)-mediated superparamagnetic graphene oxide nanocomposite called MGON, consisting of PG-modified superparamagnetic iron oxide nanoparticles (SPION) covalently bonded to PG-functionalized graphene oxide (GO). MGON exhibits better dispersibility and colloidal stability in aqueous solution than the magnetic graphene oxide reported in the literature. The physicochemical properties of MGON were analyzed by X-ray diffraction (XRD), Fourier transform infrared spectroscopy (FTIR), X-ray photoelectron spectroscopy (XPS), transmission electron microscopy (TEM), vibrating sample magnetometer (VSM), and UV-vis spectroscopy. Applied to the adsorption of tetracycline (TC) in aqueous solution as an adsorbent, the MGON showed excellent adsorption performance with the maximum adsorption capacity of 684.93 mg/g at 298 K. Adsorption kinetics and isotherm results indicate that the adsorption process conforms to the pseudo-second-order kinetics and Langmuir isotherm models. Adsorption thermodynamics has confirmed that the adsorption process of TC on MGON is spontaneous and endothermic. With the increase of temperature, the adsorption capacity of MGON increases continuously, and the adsorption capacity of MGON is the largest when the pH value is 7. Furthermore, the π-π and cation-π interaction, amidation reaction, and hydrogen bonding can be used to explain the adsorption mechanism of TC on MGON. Desorption and regeneration experiments showed that MGON still had 67.65% regenerative performance after five cycles. Hence, MGON is a promising adsorbent in the removal of tetracycline from wastewater.

Keywords Polyglycerol · Covalently bonded · Graphene oxide nanocomposite · Tetracycline · Adsorption

Introduction

Antibiotics have good inhibition and killing effects on bacteria, viruses, parasites, etc. and have good control and therapeutic effects on common diseases in daily life. Therefore, antibiotics have become more and more widely used in people's lives and become common drugs (Wammer et al. 2011). However, due to the non-standard use of antibiotics and not yet strictly regulated, it has caused the abuse of antibiotics (Bu et al. 2016; Wang et al. 2016). Especially in the medical and aquaculture industries, the abuse of drug antibiotics is particularly serious (Martínez et al. 2015), which will not only endanger human health but also cause damage to the ecosystem (Robert et al. 2013; Xie et al. 2016; Zhang et al. 2019b). Hence, it is important to develop a cost-effective adsorbent for the removal of antibiotics. Currently, the most commonly used methods for removing antibiotics are adsorption, photocatalytic degradation, biodegradation, oxidation, and electrodegradation (Gadipelly et al. 2014). Adsorption is the easiest, most economical, and most promising method of antibiotic removal for economic and environmental reasons (Álvarez-Torrellas et al. 2016; Song et al. 2014). Because of its high specific surface area, abundant surface groups, and high stability, carbon materials are preferred materials for adsorption of antibiotics, such as activated carbon, carbon nanotubes, porous carbon, and graphene (Martins et al. 2015; Xie et al. 2016; Yuan et al. 2012; Zhang et al. 2015).

Graphene is a unique two-dimensional carbon nanomaterial consisting of a single layer of carbon atoms and a sp^2 hybrid orbital hexagonal honeycomb structure. It

Responsible editor: Tito Roberto Cadaval Jr

✉ Xiulan Cai
caixiulan78@126.com

[1] Guangdong Engineering & Technology Research Center of Topic Precise Drug Delivery System, School of Pharmacy, Guangdong Pharmaceutical University, Guangzhou 510006, Guangdong, China

is expected to have a revolutionary impact in a wide range of fields on account of its excellent optical, electrical, and mechanical properties (Geim 2009; Liu et al. 2017; Rao et al. 2010). Graphene oxide has great application potential in the field of adsorption on account of its high specific surface area and a variety of hydrophilic oxygen-containing functional groups such as carboxyl and hydroxyl groups on the surface (Li et al. 2017b; Lin et al. 2013; Mukherjee et al. 2016; Yang et al. 2017b). Graphene oxide is difficult to be separated after being dispersed in water. In order to improve the separation efficiency, magnetic separation technology has attracted the interest of researchers (Han et al. 2016; Tang et al. 2012). In particular, Fe_3O_4 nanoparticles have attracted extensive attention due to their excellent properties such as low toxicity, magnetic responsiveness, outstanding superparamagnetism, and easy separation (Gong et al. 2019; Yang et al. 2017a). Fe_3O_4 nanoparticles can be introduced into common adsorbent materials such as mesoporous carbon (Yang et al. 2018a), graphene oxide (Li et al. 2018), mesoporous silica (Wang et al. 2017), and metal organic framework (MOF) (Han et al. 2019) to prepare a series of magnetic porous materials and used as adsorbents to remove contaminants. In addition, Fe_3O_4 nanoparticles can also be easily grafted with polymers such as PG, and PG-modified Fe_3O_4 nanoparticles are not only easier to further functionalize, but also increase their dispersion stability and biocompatibility in water (Zhao et al. 2012).

Recently, PG has become a commonly used surface modifier because of its excellent physical and chemical properties (Li et al. 2011; Yang et al. 2018a, b). The PG layer can be grafted directly onto nanomaterials with reactive functional groups such ascarboxyl and hydroxyl groups by a "grafting" method of in situ ring-opening polymerization initiated by glycidol (Mohsen et al. 2009; Yang et al. 2017a). PG-functionalized nanomaterials have high hydrophilicity, good dispersibility, and biocompatibility in aqueous media. Furthermore, by stepwise organic reactions, the hydroxyl groups on the PG layer can be easily converted to more reactive functional groups such as carboxyl, amino, and azide groups to facilitate further functionalization (Yang et al. 2019). Based on the above strategies, Yang et al. reported the application of polyglycerol-mediated nuclear-satellite superparamagnetic mesoporous carbon nanocomposites in dye adsorption (Yang et al. 2018a). But so far, the preparation of covalently bonded superparamagnetic graphene oxide nanocomposites by two PG layers has not been reported.

In this paper, we successfully prepared a polyglycerol-mediated superparamagnetic graphene oxide nanocomposite by constructing a strategy that covalently mediates PG linkage. Applied to the removal of tetracycline in aqueous solution, and the effects of adsorption time such as contact time, temperature, solution pH, and ionic strength were investigated. At the same time, the isotherms, kinetics, and thermodynamics of the adsorption process were studied, and the adsorption mechanism of MGON on TC was also discussed.

Materials and methods

Materials

Graphene was purchased from Suzhou Carbon Graphene Technology Co., Ltd. Sulfuric acid and nitric acid were supplied by Guangzhou Chemical Reagent Factory, China. Glycidol (96%) and triethylene glycol (98%) were purchased from Aladdin. N-Hydroxysuccinimide (NHS) (98%), 1-(3-dimethylaminopropyl)-3-ethylcarbodimide hydrochloride (EDC) (98.5%), ethylenediamine dihydrochloride, 4-dimethylaminopyridine (DMAP) (99%), tetracycline hydrochloride (USP), and iron(III) acetylacetonate (98%) were provided by Mackin. Ethyl acetate, pyridine, and methanol were obtained by Tianjin Zhiyuan Chemical Reagent Co. Ltd. All chemicals were used without further purification.

Characterization

The FTIR spectrum was collected at room temperature by a Nicolet iS50 FTIR spectrometer (Thermo Scientific). XRD pattern was carried out on a Bruker D8 Advance X-ray diffractometer with Cu Kα irradiation operated at 40 mA and 40 mA, and TEM was conducted on a FEI Tecnai G2 Spirit BioTWIN apparatus with an acceleration voltage of 120 kV. XPS measurements were measured using a Thermo Escalab 250Xi instrument and UV–vis absorption spectroscopy on a Shimadzu UV-3600 spectrophotometer. The magnetic properties of sample were examined with a magnetic field of ± 10,000 KOe at 27 °C by VSM.

Synthesis of GO, GO-PG, and GO-PG-COOH

One hundred milligrams of graphene was added to 60 mL of mixed acid (concentrated sulfuric acid/concentrated nitric acid = 3:1) and sonicated for 1 h. The reaction was stirred under reflux at 60 °C for 8 h. After the reaction was completed, it was cooled to room temperature, and the product was centrifuged five times at 4000 rpm to obtain GO reserve liquid.

Ten milliliters of glycidol was added to 200 mg dried GO and sonicated to completely disperse. Then, the reaction was stirred at 140 °C for 24 h. After the reaction was over, cooled to room temperature, and an appropriate amount of deionized water was added to ultrasonically disperse it. Finally, the product GO-PG was obtained by multiple ultrafiltration washing (MWCO = 100 K, Amicon, Millipore) and stored at 4 °C before being used.

The GO-PG reaction solution was evaporated to dryness and dissolved in an appropriate amount of pyridine. Succinic anhydride and DMAP (succinic anhydride: GO-PG = 2:1; DMAP: GO-PG = 1:1) were then added, and the reaction was stirred magnetically for 24 h at room temperature. After the reaction, the mixed solution is dialyzed in water to remove pyridine, unreacted succinic anhydride, and free DMAP, then ultrafiltered twice with methanol/water (*v*/*v* = 1:1), and finally ultrafiltered three times with deionized water to acquire GO-PG-COOH reserve liquid.

Synthesis of SPION-PG-NH_2

SPION-PG-COOH was synthesized in terms of the method previously reported (Yang et al. 2017a). To introduce amino groups, 1 mg EDC and 10 mg NHS were dissolved in 2 mL 5 mg/L SPION-PG-COOH solution and stirred for 1 h to activate the carboxyl group, and then 20 mg ethylenediamine hydrochloride was added and the reaction was stirred magnetically at room temperature for 24 h. After the reaction finished, the product was subjected to ultrafiltration multiple times to obtain SPION-PG-NH_2 stock solution.

Synthesis of MGON

Fifteen milligrams NHS and 1.5 mg EDC were added to 3 mL 5 mg/L GO-PG-COOH solution and stirred for 1 h to activate the carboxyl group, after which 5 mg SPION-PG-NH_2 was added. Then, the mixture was magnetically stirred for 24 h at room temperature. After the reaction was completed, the product was washed multiple times to obtain MGON nanocomposite.

Adsorption experiment

All batch adsorption experiments were conducted in 20 mL brown glass vials by adding 4.5 mg MGON to 15 mL 30 mg/L TC solution and shaking for 24 h at a speed of 150 rpm. In order to inquire the kinetics of adsorption, 4.5 mg MGON was added to different tetracycline concentrations (0–500 mg/L) (pH = 7) to evaluate the effect of different TC concentrations on adsorption. At the same time, we also studied the effects of different temperature conditions (288 K, 298 K, 308 K) and different NaCl concentrations on the adsorption of tetracycline by MGON. Then, MGON was removed by using a magnet, and the tetracycline concentration before and after adsorption was examined by a UV-vis-NIR absorption spectrum at a maximum absorption wavelength of 358 nm.

To further investigate the regeneration and reusability of MGON, we performed desorption experiments. The regeneration of MGON was carried out by adding MGON/TC to a 0.01 M NaOH solution (400 mL), and the mixture was stirred at 25 °C for 24 h. Repeat the same procedure five times and separate the solid/liquid phase by a magnet. In each adsorption cycle, the suspension liquid containing 4.5 mg MGON and 30 mg/L TC (150 mL) was shaken at 25 °C for 24 h at a pH of 7.

The amount of adsorption was determined by using the following formula:

$$q_e = \frac{(C_0 - C_e)V}{m_{MGON}} \tag{1}$$

where q_e (mg/g) is the adsorption amount at equilibrium; C_0 and C_e (mg/L) are the initial concentration and equilibrium concentration of TC in solution, respectively; V (L) is the volume of solution; m_{MGON} (g) is the mass of the adsorbent used.

Models of data analysis

To investigate the adsorption mechanism and identify potential rate control steps, the pseudo-first-order, the pseudo-second-order, and the Boyd membrane diffusion models were employed to analyze experimental data (Li et al. 2017b).

The pseudo-first-order model:

$$In(q_e - q_t) = In\, q_e - k_1 t \tag{2}$$

The pseudo-second-order model:

$$\frac{t}{q_t} = \frac{t}{q_e} + \frac{1}{q_e^2 k_2} \tag{3}$$

The Boyd's film-diffusion model:

$$B_t = -0.4977 - In(1 - F) \tag{4}$$

where q_e and q_t are severally the adsorbed amount of tetracycline at equilibrium and at different time (mg/g). k_1, k_2 are the adsorption rate constants of the pseudo-first-order and the pseudo-second-order models, respectively. B_t is mathematical function of F, and F is equivalent to q_t/q_e (Yang et al. 2017b).

In order to study the adsorption efficiency, the adsorption process of tetracycline was analyzed by Langmuir, Freundlich, and Temkin isotherm models, which were expressed in Eqs. (5), (6), and (7), respectively, as follows (Gao et al. 2012):

The Langmuir isothermal model:

$$\frac{C_e}{q_e} = \frac{C_e}{q_m} + \frac{1}{q_m K_L} \tag{5}$$

The Freundlich isothermal model:

$$In\, q_e = In\, K_F + \frac{1}{n} In\, C_e \tag{6}$$

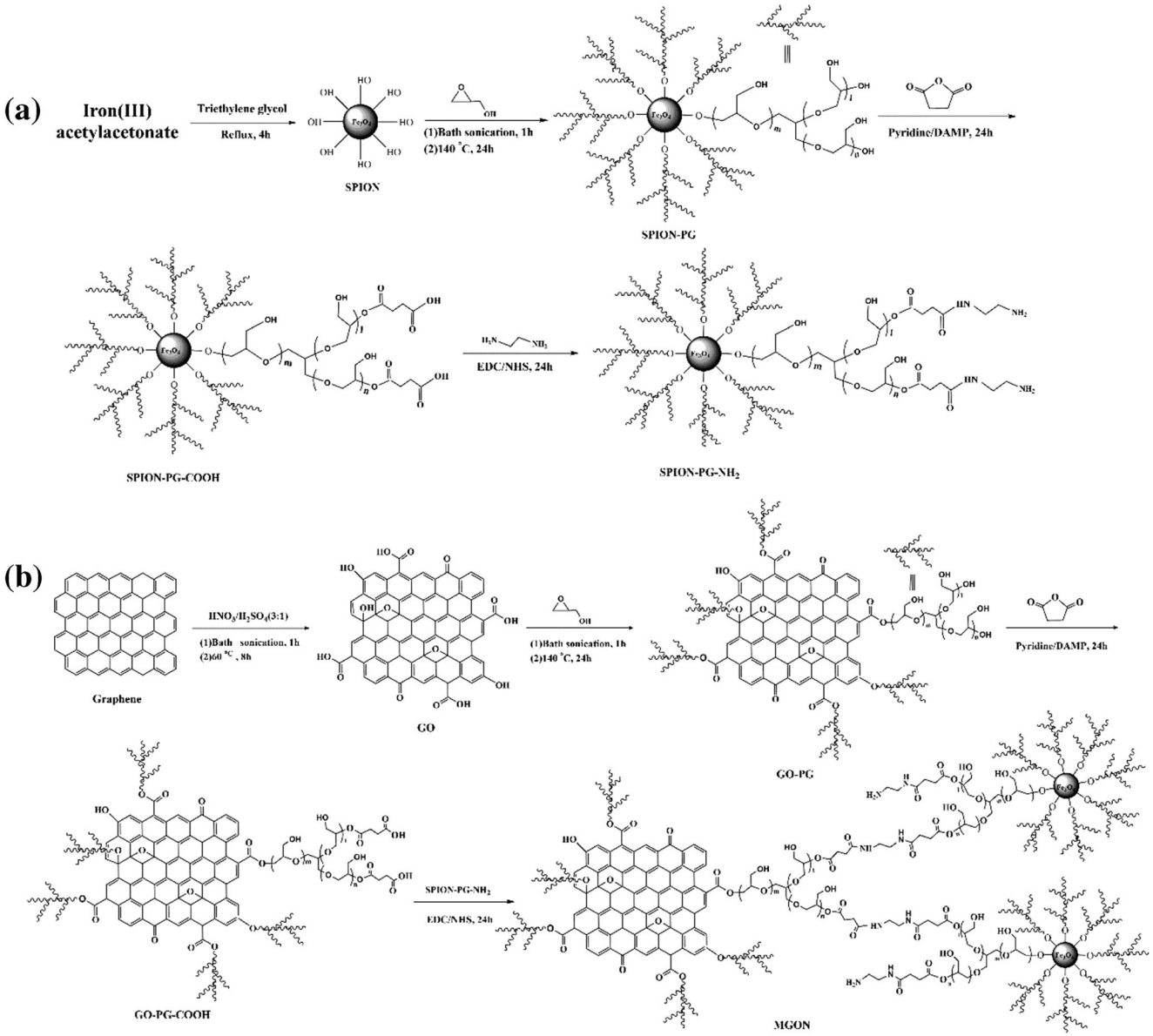

Scheme 1 **a** Synthesis steps of SPION-PG-NH_2. **b** The preparation steps of MGON

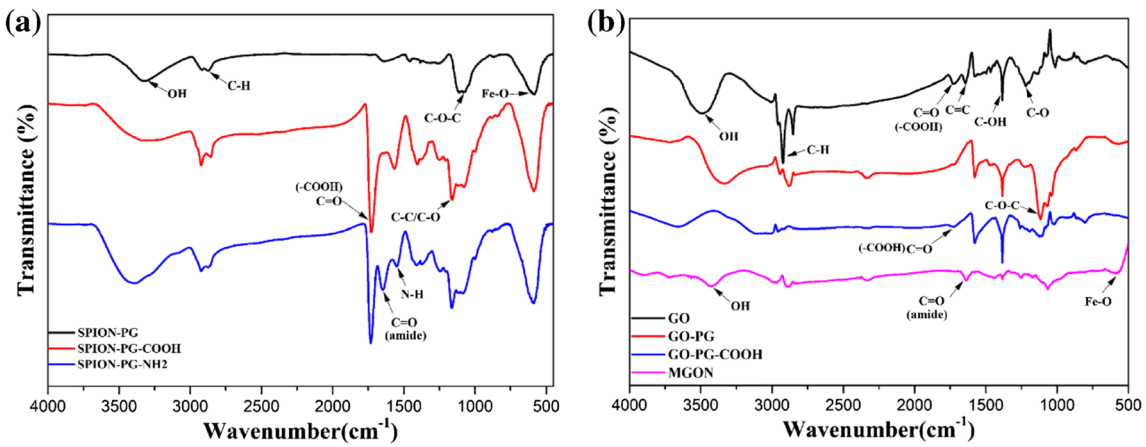

Fig. 1 FTIR spectra of **a** SPION-PG, SPION-PG-COOH, and SPION-PG-NH_2. **b** GO, GO-PG, GO-PG-COOH, and MGON

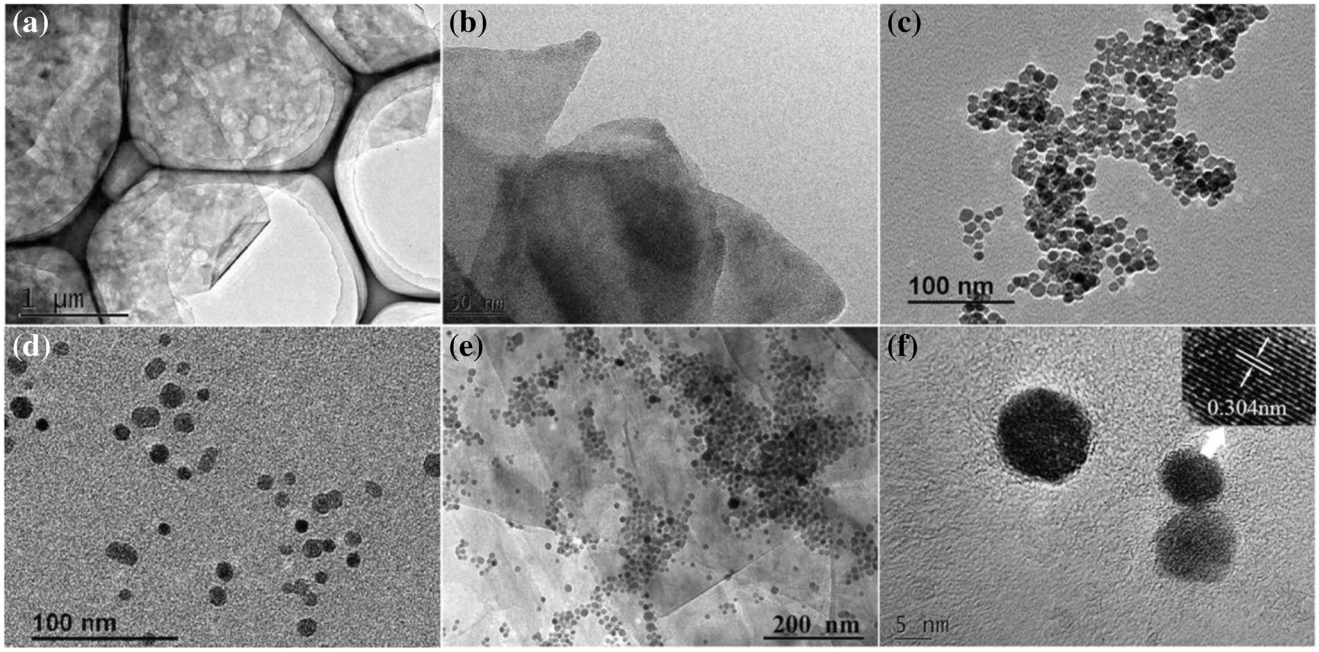

Fig. 2 TEM images of **a** GO, **b** GO-PG, **c** SPION, **d** SPION-PG, and **e** MGON. **f** HRTEM image of MGON

The Temkin isothermal model:

$$q_e = K_T In\, C_e + K_T In\, f \tag{7}$$

where $q_e$and q_m are the equilibrium-absorbed concentration and the maximum adsorption capacity of the adsorbent (mg/g), respectively. C_e (mg/L) is the equilibrium solution phase concentration and n is the Freundlich linearity index. K_L, K_F, K_T are severally the adsorption constants of Langmuir, Freundlich, and Temkin isotherm models.

Adsorption thermodynamics is useful for understanding the extent and driving force of the adsorption process and revealing the mechanism in the adsorption process. The adsorption thermodynamic parameters are obtained by the following formula (Zhang et al. 2019b):

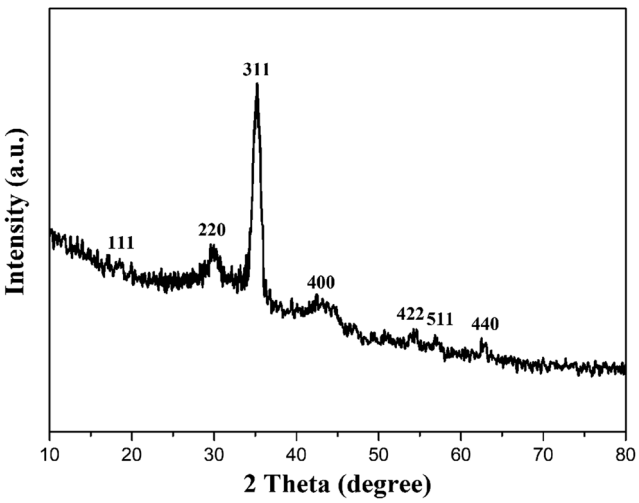

Fig. 3 XRD pattern of MGON

$$\Delta G^{\theta} = -RT{\cdot}In\, K_0 \tag{8}$$

$$In\, K_0 = \frac{-\Delta H^{\theta}}{R} \times \frac{1}{T} + \frac{\Delta S^{\theta}}{R} \tag{9}$$

$$\Delta G^{\theta} = \Delta H^{\theta} - T{\cdot}\Delta S^{\theta} \tag{10}$$

where ΔG^{θ}(KJ·mol-1), ΔS^{θ}(J/(mol·K)), and ΔH^{θ}(KJ/mol) are adsorption thermodynamic constants, which represent entropy change, enthalpy change, and Gibbs free energy change, respectively. R is an ideal gas constant (8.314 J/(mol·K)). K_0 is the adsorption equilibrium constant and is equivalent to $q_m \times K_L$ (L/g).

Results and discussion

The synthesis strategy of MGON is delineated in Scheme 1. SPION synthesized by thermal decomposition was grafted with PG in terms of reported methods before. The grafted PG layer not only improves the hydrophilicity but also provides a rich hydroxyl group for further modification (Yang et al. 2019, 2018b). SPION-PG-COOH was prepared by reacting SPION-PG with succinic anhydride. Next, SPION-PG-COOH is reacted with ethylenediamine, and an amino group is introduced on the surface to acquire SPION-PG-NH_2. Graphene oxide is produced by oxidation of graphene by mixed acid (Jia et al. 2013), and then grafted with PG. The GO-PG is reacted with succinic anhydride to form a carboxyl group on the surface to obtain GO-PG-COOH. Finally, MGON was synthesized by amidation reaction of GO-PG-COOH and SPION-PG-NH_2 under the activation of NHS/

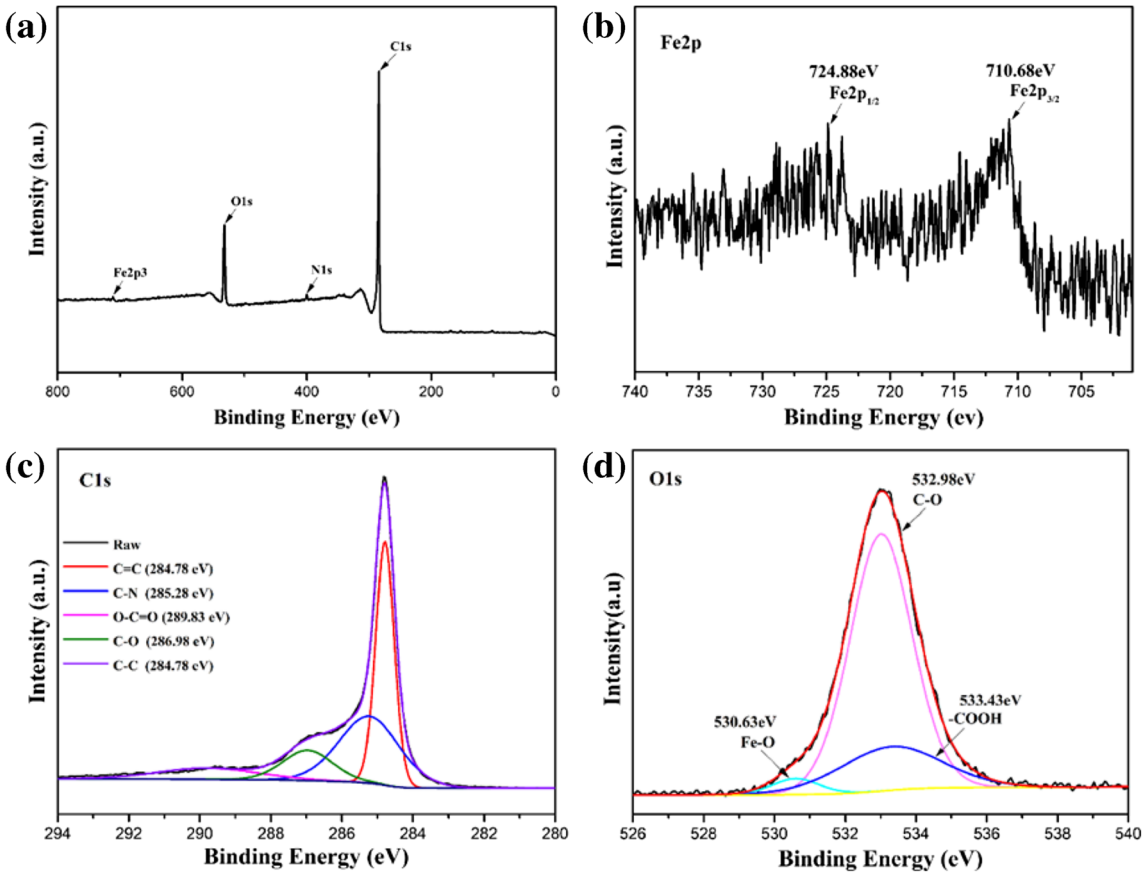

Fig. 4 Typical XPS results of MGON samples. **a** Full spectrum. Core level spectra of **b** Fe 2p, **c** C 1s, and **d** O 1s

EDC. The various characterization methods for detecting the synthetic process by the following methods are as follows.

Characterization

The FTIR spectroscopy is a crucial method for qualitative analysis of the characteristic peaks of materials, whose chemical structure can be studied. The FTIR patterns of SPION, SPION-PG, SPION-PG-COOH, and SPION-PG-NH_2 are shown in Fig. 1a. The increase of the absorption bands at 1085, 2915, and 3402 cm^{-1} severally correspond to the stretching vibrations of C-O-C, C-H, and O-H, which indicates that PG was successfully grafted on SPION (Zhao et al. 2012). The strong peak at 1726 cm^{-1} confirmed the existence of carboxylic acid groups on the surface of SPION-PG after modification, and the peak at 1163 cm^{-1} is attributed to coupled C-C/C-O stretch vibration (Badruddoza et al. 2011). In the spectra of SPION-PG-NH_2, the two characteristic absorbance bands centered at 1645 cm^{-1} and 1555 cm^{-1} which can be attributed to the C=O stretching

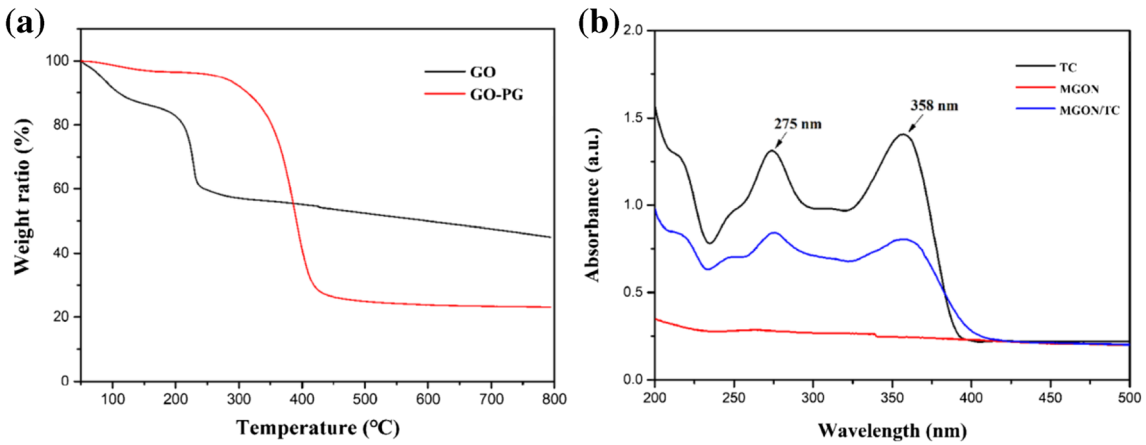

Fig. 5 **a** TGA curves of GO and GO-PG under nitrogen. **b** UV-vis absorption spectra of MGON, TC, and MGON/TC

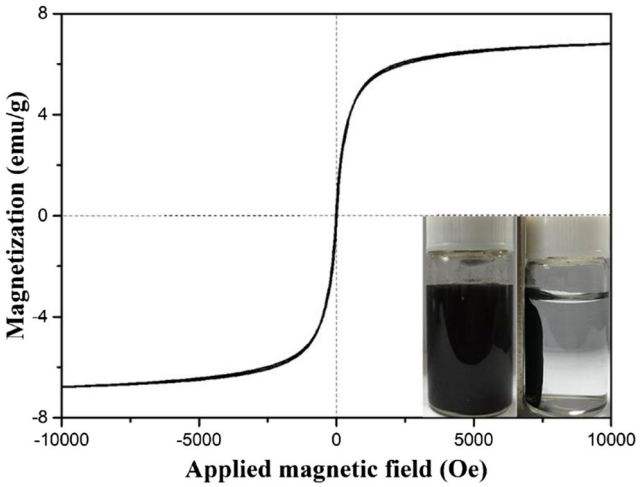

Fig. 6 Magnetization curve of MGON hybrid. The bottom insert displayed dispersed MGON nanocomposites and magnetic separation

vibration of -NHCO- (amide) and the N-H bending of NH_2, respectively (Yang et al. 2018a). Figure 1b shows the FTIR spectra of GO, GO-PG, GO-PG-COOH, and MGON. The absorption bands of GO appeared at 3475, 2923, 1725, 1642, 1385, and 1210 cm^{-1} correspond to O-H, C-H, C=O (carboxylic acid groups), C=C, C-OH, and C-O stretching vibrations, respectively (Li et al. 2017a; Yao et al. 2012). The increasing absorption band at 1100 cm^{-1} (C-O-C stretching vibration) means that PG is successfully grafted on the surface of GO (Yang et al. 2019), which is also supported by TGA result (Fig. 5a), The result indicated that the graft amount of PG was about 21.88 wt% at 200~800 °C. The absorbance peak at 1728 cm^{-1} correspond to C=O stretching vibration of carboxylic acid groups in the FTIR curve of GO-PG-COOH. After conjugation with SPION-PG-NH_2, the characteristic absorption band at 1635 cm^{-1} is attributed to the C=O stretching vibration of -NHCO- (amide I) in the FTIR spectrum of MGON (Fan et al. 2012). Furthermore,

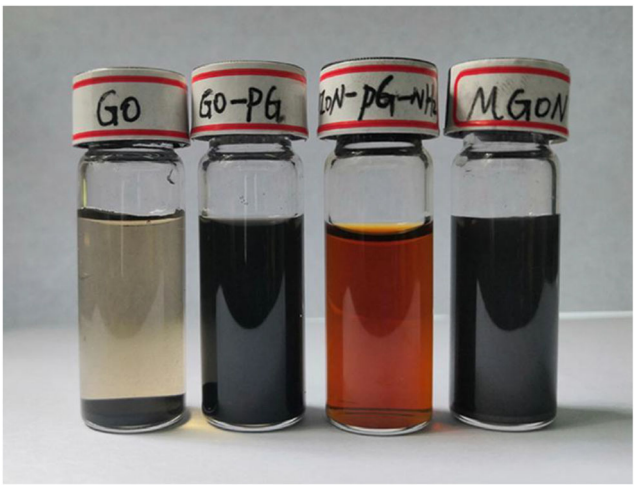

Fig. 7 The dispersion stability of GO, GO-PG, SPION-PG-NH_2, and MGON in aqueous solution

580 cm^{-1} is a characteristic absorption peak of Fe_3O_4 (Wang et al. 2019). These results indicated that MGON was successfully prepared.

Figure 2 shows typical TEM images and size distribution of GO, GO-PG, SPION, SPION-PG, and MGON. It can be seen from Fig. 2a that GO showed a folded layered structure and was partially transparent, suggesting that the thin layer of the base which may support a higher surface area-to-volume ratio to provide more active sorption sites for the target contaminant (Cui et al. 2015). The morphology of GO-PG is shown in Fig. 2b. After PG was chemically grafted on the surface of GO, a more pronounced dark region was observed, which was related to the grafted PG on the surface of GO. This speculation can also be confirmed from Fig. 5a. The dark areas on the GO base surface indicate a higher density of grafted PG, which can be explained by the higher density of hydroxyl functional groups on the GO surface (Pham et al. 2010). Good shape ellipsoidal or nearly spherical SPION were observed with an average size of about 12.06 nm in Fig. 2c. The SPION-PG-NH_2 shown in Fig. 2d has high dispersibility and stability in aqueous solution. Figure 2 e demonstrates the fixation of SPION on GO. It can be observed that a large number of nanoparticles are in the darker color region, while the lighter color region has only a small amount of nanoparticles, indicating that SPION are immobilized on the surface of the GO-PG by a strong covalent bond of the amide bond, rather than by simple physical absorption or hydrogen bond interaction. The HRTEM image (Fig. 2f) showed that the SPION were strongly attached onto the GO nanosheets. The well-resolved lattice fringes with an interplane spacing of 0.304 nm are attributed to the d-spacing of the (220) planes of Fe_3O_4, which agrees with the XRD results, attesting the formation of well-textured and highly crystalline SPION in MGON (Xie et al. 2011).

The XRD pattern was used to characterize the crystal structure of MGON. Figure 3 shows characteristic diffraction peaks at 18.50, 29.93, 35.45, 43.23, 53.85, 57.14, and 62.91 (2θ), which was well matched with the standard materials (JCPDS 19-0629) (Li et al. 2017b). The results revealed that Fe_3O_4 nanocrystals are highly crystallized in MGON (Lian et al. 2016).

The elemental composition and surface chemical valence states of MGON were further analyzed by XPS. The wide-scan XPS full spectrum of MGON in Fig. 4a showed four peaks at 284.08, 400.48, 532.08, and 711.08 eV corresponding to C 1s, N 1s, O 1s, and Fe 2p, respectively. Figure 4b exhibits the high-resolution XPS spectrum of Fe 2p, and the two peaks centered at binding energies of 710.68 and 724.88 eV are severally assigned to Fe $2p_{3/2}$ and Fe $2p_{1/2}$, which is very consistent with the reported values for Fe_3O_4 (Lei et al. 2014). The core level spectrum of C 1s (Fig. 4c) displayed four component peaks at binding energies of 284.78, 285.28, 286.98, and 289.83 eV corresponding to

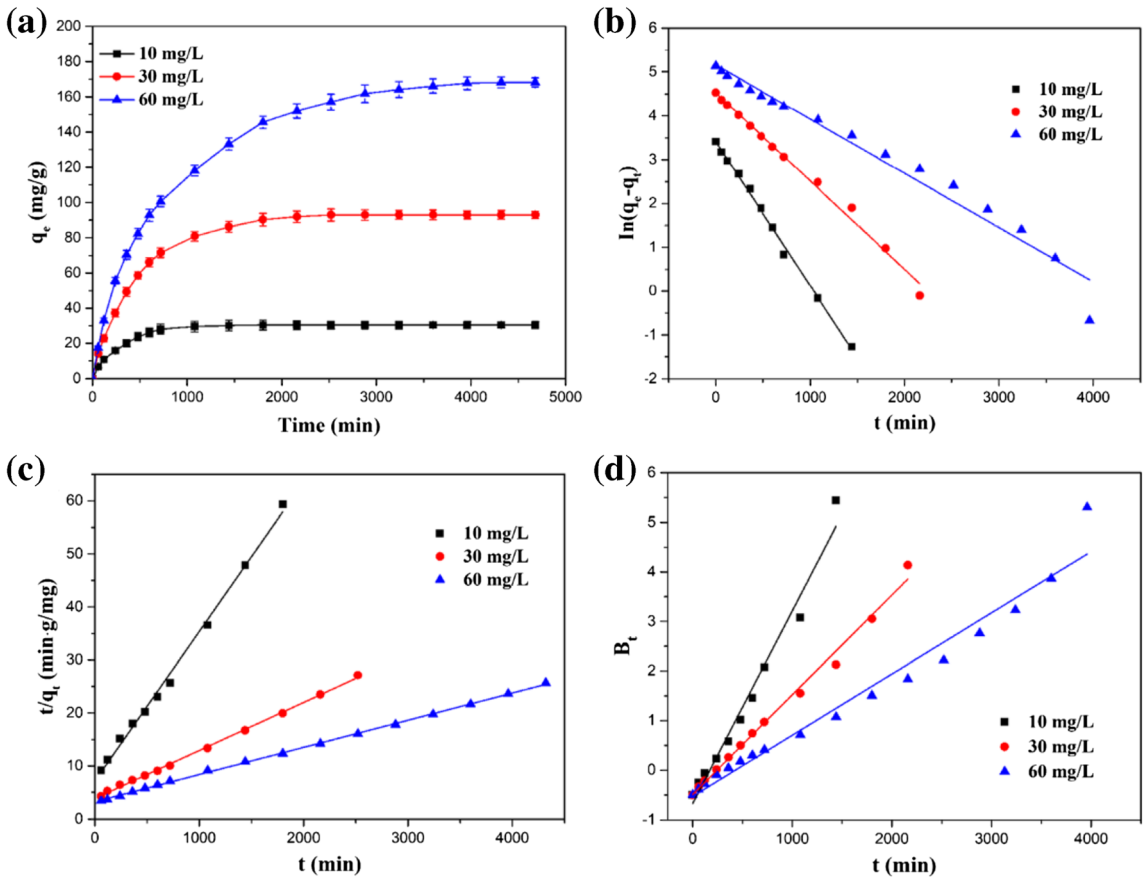

Fig. 8 **a** Adsorption kinetics of tetracycline onto MGON. **b** Pseudo-first-order kinetics. **c** Pseudo-second-order kinetics. **d** Boyd's film-diffusion kinetics. C_{MGON} = 0.3 mg/mL, T = 25 °C, pH = 7.0

C=C/C-C, C-N, C-O, and O-C=O groups, respectively (He et al. 2010; Li et al. 2017b). As shown in Fig. 4d, the high-resolution spectrum of O 1s can be disintegrated into three peaks at binding energies of 530.63, 532.98, and 533.43 eV, which severally belong to Fe-O, C-O (alcoholic hydroxyl and ether), and C=O groups (Badruddoza et al. 2011; Lei et al. 2014). These results further demonstrate that MGON has been successfully synthesized.

The UV–vis absorption spectra of MGON, TC, and MGON/TC are displayed in Fig. 5b. It can be clearly seen that the spectrum of MGON has almost no characteristic absorption peaks and TC has two strong absorption peaks at 275 nm and 358 nm, while the absorption spectra of MGON/TC also displays two absorption peaks at 275 nm and 358 nm. The results demonstrated that tetracycline was successfully adsorbed on the MGON surface.

Table 1 Kinetics parameters for adsorption of tetracycline onto MGON

Models	Parameter	C_0 (mg/L)		
		10.00	30.00	60.00
Pseudo-first-order model	$q_{e.cal}$ (mg/g)	30.30	92.54	174.13
	k_1 (/min)	0.00329	0.00201	0.00124
	R^2	0.9967	0.9920	0.9695
Pseudo-second-order	$q_{e.cal}$ (mg/g)	35.46	109.89	196.08
	k_2 (g/mg min)	1.11×10^{-4}	2.15×10^{-5}	8.00×10^{-6}
	R^2	0.9959	0.9987	0.9994
Boyd's film diffusion	Intercept	− 0.6746	− 0.494	− 0.5305
	Slope	0.00389	0.00201	0.00124
	R^2	0.9786	0.9919	0.9694

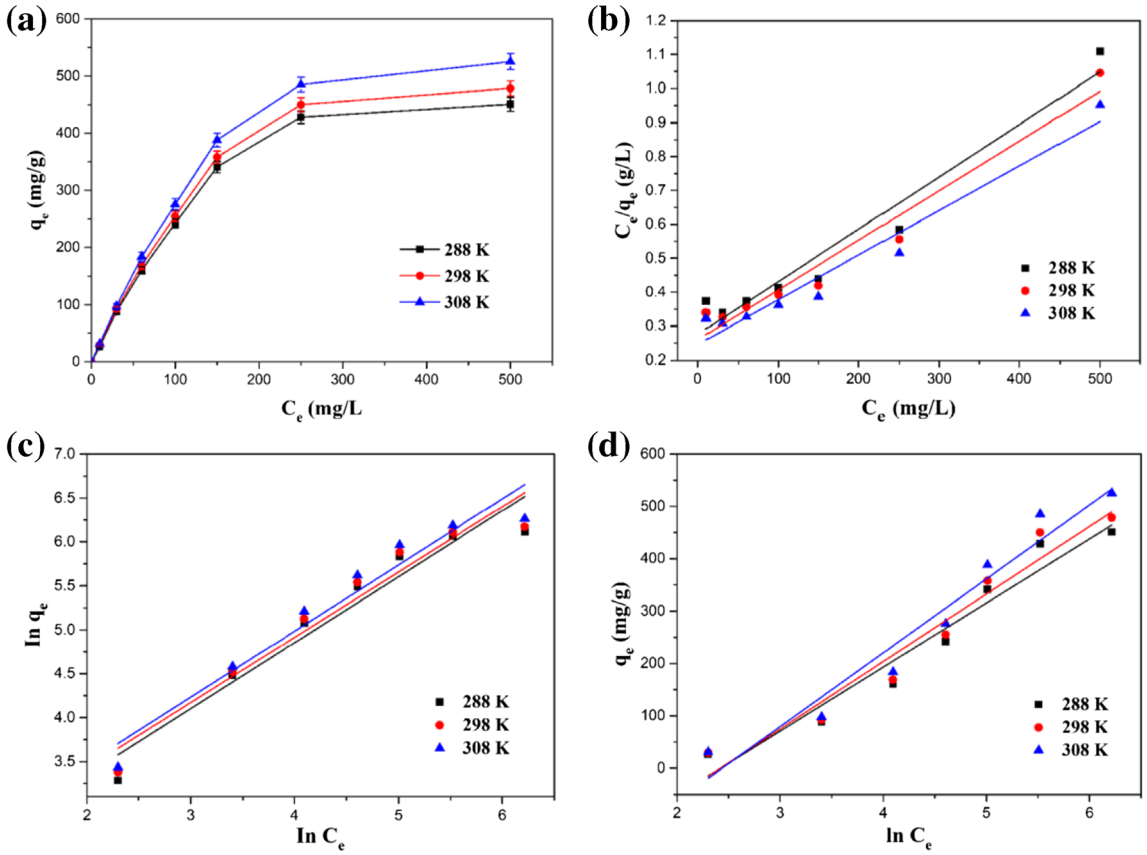

Fig. 9 **a** Adsorption isotherms of tetracycline onto MGON. **b** Langmuir, **c** Freundlich, and **d** Temkin model fitting for the adsorption of TC onto MGON. C_{MGON} = 0.3 mg/mL, pH = 7.0

As shown in Fig. 6, the magnetization property of the MGON was conducted at room temperature by VSM. The saturation magnetization of MGON was measured to be 6.81 emu/g. The saturation magnetization of the MGON mixture we synthesized is smaller than that reported in some literature (Cui et al. 2015; Huang et al. 2017). This decrease can be attributed to the smaller size of Fe_3O_4 nanoparticles, the surface modification of PG to Fe_3O_4, and the presence of GO (He et al. 2010; Yang et al. 2018a). The magnetized hysteresis loop exhibits an S-like curve and the magnetic coercivity or remanence is almost zero, suggesting the superparamagnetic behavior of MGON (He et al. 2010). In addition, as shown in Fig. 6 (bottom inset), MGON can achieve solid-liquid separation in a few minutes under the action of external magnetic force. The one on the left exhibited the MGON was nicely decentralized in aqueous solution, while the one on the right displayed how the MGON was separated via placing a magnet near the container. The photograph in Fig. 7 shows the

Table 2 Isotherm parameters for adsorption of tetracycline onto MGON

Models	Parameters	T (K)		
		288	298	308
Langmuir	q_{max} (mg/g)	649.35	684.93	757.58
	K_L (L/mg)	5.57×10^{-3}	5.61×10^{-3}	5.35×10^{-3}
	R^2	0.9507	0.9584	0.9570
Freundlich	K_F (L/mg)	6.3509	6.9594	7.1965
	n	1.3316	1.3454	1.3287
	R^2	0.9417	0.9456	0.9468
Temkin	K_T	141.12	129.03	122.38
	R^2	0.9514	0.9492	0.9490

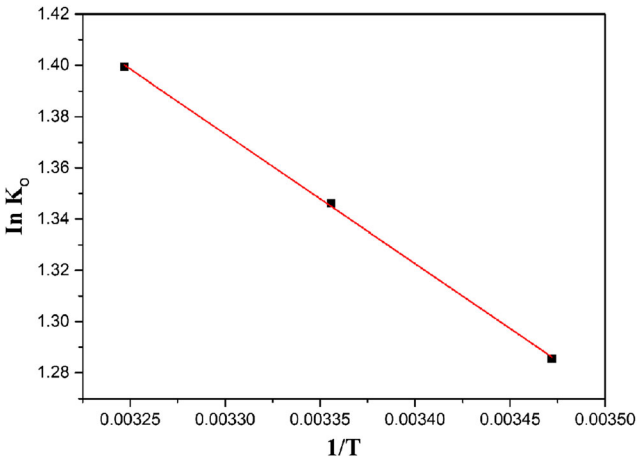

Fig. 10 Adsorption thermodynamics of TC adsorption on MGON

Table 3 Adsorption thermodynamic parameters of tetracycline on MGON

T (K)	K_0	ΔH^0 (KJ/mol)	ΔS^0(J/(mol/K))	ΔG^0 (KJ/mol)
288	3.6169	4.2101	25.3103	− 3.0792
298	3.8425			− 3.3323
308	4.0531			− 3.5854

dispersion stability of GO, GO-PG, SPION-PG-NH_2, and MGON with a concentration of 2 mg/L in aqueous solution. It was observed that the GO sample formed a distinct precipitate at the bottom of the bottle within 10 h, while the GO-PG and SPION-PG-NH_2 samples hardly changed, which proved that GO-PG and SPION-PG-NH_2 exhibited excellent dispersion and colloidal stability in the aqueous solution, and could maintain good dispersion stability for a long time. In addition, MGON, which is covalently synthesized by polyglycerol can also maintain a well-dispersed state in water.

Adsorption kinetics

Adsorption is a physicochemical process concerning the mass transfer of solutes from the liquid phase to the surface of the adsorbent (Hu et al. 2011). Adsorption kinetics is a significant parameter to depict the adsorption rate of adsorbate at the solid-liquid interface. The adsorption kinetics of the whole adsorption process was studied to fully illustrate the influence of adsorption rate and adsorption time, which is helpful to understand the adsorption behavior of MGON. Figure 8a shows the time profile of different initial concentrations of TC adsorbed from aqueous solution onto MGON. It can be seen from the adsorption process that the higher the original concentration of TC is, the longer the reaction takes to reach the adsorption balance. The removal rates of TC solutions with initial concentrations of 10 mg/L, 30 mg/L, and 60 mg/L within 24 h are 90.24%, 86.18%, and 66.62%, respectively. Moreover, it can be observed that the adsorption capacity of MGON increases rapidly within the first hour, and then slowly increases until the adsorption equilibrium is reached. To further investigate the adsorption mechanism and describe the kinetics of MGON adsorption of TC, the pseudo-first-order and the pseudo-second-order models were applied. The kinetic parameters in the two models in Table 1 are derived from Eqs. (1), (2), and (3). The comparison of the correlation coefficient (R^2) shows that the R^2 value (0.9959, 0.9987, 0.9994) of the pseudo-second-order rate model is larger than the R^2 value (0.9967, 0.9920, 0.9695) of the pseudo-first-order model, and the obtained $q_{e,\ cal}$ value is closer to the $q_{e,\ exp}$ value. These indicate that the chemistry adsorption dominates the adsorption of tetracycline by MGON and the pseudo-second-order kinetic model can better explain the adsorption behavior of TC on MGON.

To clarify the step of controlling the total elimination rate of the adsorption process, the Boyd's film-diffusion model is used in the adsorption of tetracycline (Fig. 8d). Based on in light of Eq. (4), for a linear plot of B_t versus t through the origin, the pore diffusion determines the mass transfer rate. Conversely, if the resulting plot is non-linear or linear but does not cross the origin, we can draw the conclusion that membrane diffusion or chemical reactions also make a leading role in the rate of adsorption (Yang et al. 2017b). The intercepts obtained as in Table 1 are all non-zero, foreboding that the diffusion process is controlled by means of membrane diffusion or chemical reaction.

Adsorption isotherms

The adsorption isotherm of tetracycline is shown in Fig. 9a. The adsorption capacities at 288, 298, and 309 K are 450.8, 478.43, and 525.3 mg/g, respectively. The adsorption capacity increased with the increase of the initial concentration of TC, suggesting that a higher concentration of TC was beneficial to adsorption, which may be due to the introduction of rich -NH_2

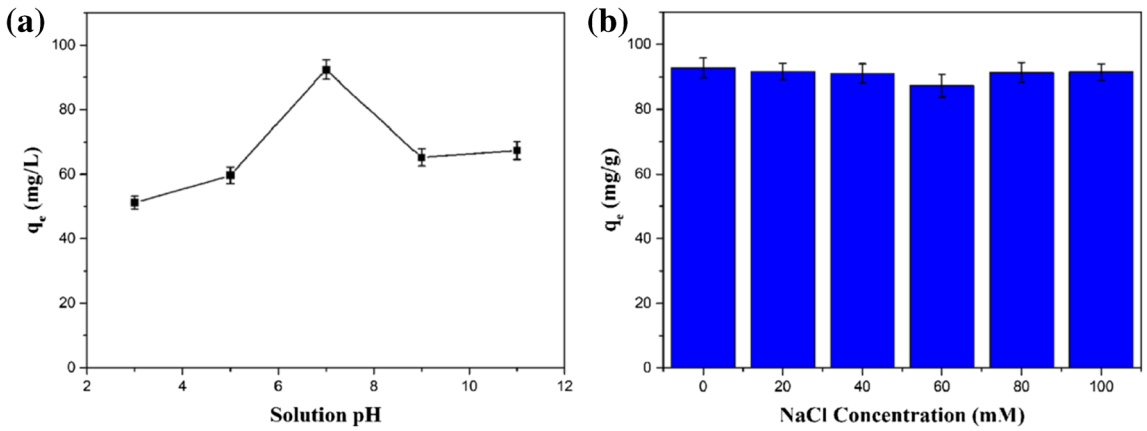

Fig. 11 Effects of pH (**a**) and ionic strength (**b**) on TC adsorption by MGON. $C_{0\ (TC)}$ = 30.0 mg/L, C_{MGON} = 0.3 mg/L, T = 25 °C

Table 4 The comparison of adsorption capacity (q_m) of various adsorbents for tetracycline

Adsorbent	Dosage (mg/mL)	pH	TC concentration (mg/L)	q_m (mg/g)	Refs.
NDMGO	0.19	4.0	150	356	Li et al. (2017b)
GO	0.181	3.6	166.67	313	Yuan et al. (2012)
MGOS	0.625	3.0	300	473	Yu et al. (2017)
MWCNTs	0.2	7.0	200	364.37	Xiong et al. (2018)
Smectite	5	4.0	1000	462	Li et al. (2010)
$CoFe_2O_4$/MMT	0.4	4.0	120	240.91	Zhang et al. (2019a)
MBC	0.4	6.0	500	177.71	Liang et al. (2019)
MCB	0.2	8.0	100	480	Oladipo and Ifebajo (2018)
MCBB	25	10.0	100	63.3	Oladipo et al. (2017)
$CoO/CuFe_2O_4$	1	6.0	200	138.6	Ifebajo et al. (2018)
MGON	0.3	7.0	500	478.43	This work

NDMGO nitrilotriacetic acid to magnetic graphene oxide, *MGOS* magnetic graphene oxide sponge, *MBC* modified biochar, *MCB* magnetic chicken bone biochar, *MCBB* magnetic chicken bone-based biochar

group to the sp^2 carbon network and MGON's large surface area. In current work, three conventional classical adsorption models, namely Langmuir, Freundlich, and Temkin models, are used to illustrate the adsorption equilibrium process. The Langmuir model is a model with ideal adsorption surface and single layer molecular adsorption. The Freundlich model is widely used in the field of chemistry as an empirical model. Temkin model is a chemical adsorption model based on strong electrostatic interaction between positive and negative charges (Yuan et al. 2012). Figure 9b–d exhibit the fitting results for the three models, and the fitting parameters are situated in Table 2. It can be seen from the comparison of the correlation coefficient (R^2) that the isotherm Langmuir model can better explain the adsorption process of TC on MGON than the Freundlich model. Therefore, single-layer adsorption dominates the adsorption process with the contribution of heterogeneous adsorption. The maximum adsorption capacities (q_m) obtained by the Langmuir isotherms at 288, 298 and 308 K were 649.35, 684.93 and 757.58 mg/g, respectively. As the temperature rises, the adsorption capacity of MGON for TC is also increasing, which demonstrates that higher temperatures is conducive to adsorption.

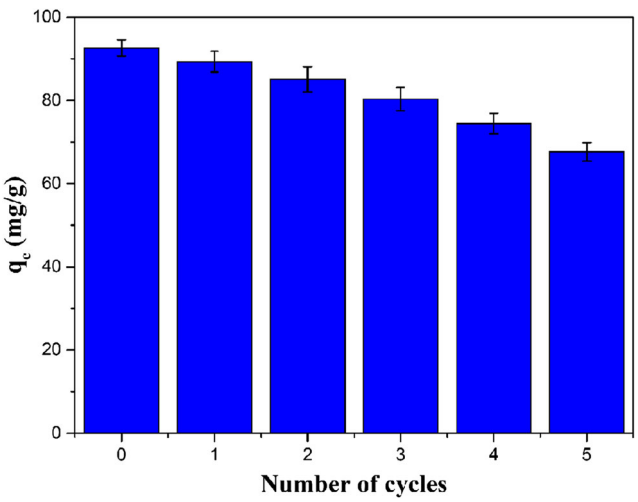

Fig. 12 Five adsorption-desorption cycles for MGON. $C_{0\ (TC)} = 30.0$ mg/L, $C_{MGON} = 0.3$ mg/L, $T = 25$ °C, pH = 7.0

Adsorption thermodynamics

In order to describe the adsorption process more clearly, the adsorption thermodynamics of TC was investigated (Fig. 10). The experimental results showed that higher temperatures favor the adsorption of TC, which may be due to the increase in temperature, the tetracycline molecules move faster in solution, increasing their chances of contact with the adsorbent. All obtained thermodynamic parameters are listed in Table 3. All ΔG^0 values calculated at various temperatures are negative, which means that the adsorption process is spontaneous (Ocampo-Pérez et al. 2012). Moreover, positive values of ΔH^0 and ΔS^0 demonstrate that the adsorption process of tetracycline on MGON is endothermic and is accompanied by an increase in entropy of the solid-liquid interface system during tetracycline adsorption.

Effects of pH and ionic strength on the adsorption of TC

The effect of pH acts a crucial role during the adsorption process, which can change the surface charge of the adsorbent, the morphology distribution, and ionization of the target compound (Oladipo and Ifebajo 2018; Oladipo et al. 2017). The impact of pH on the adsorption process is shown in Fig. 11a. The adsorption behavior of TC on MGON has a significant pH dependence. When the pH increased from 3.0 to 7.0, the

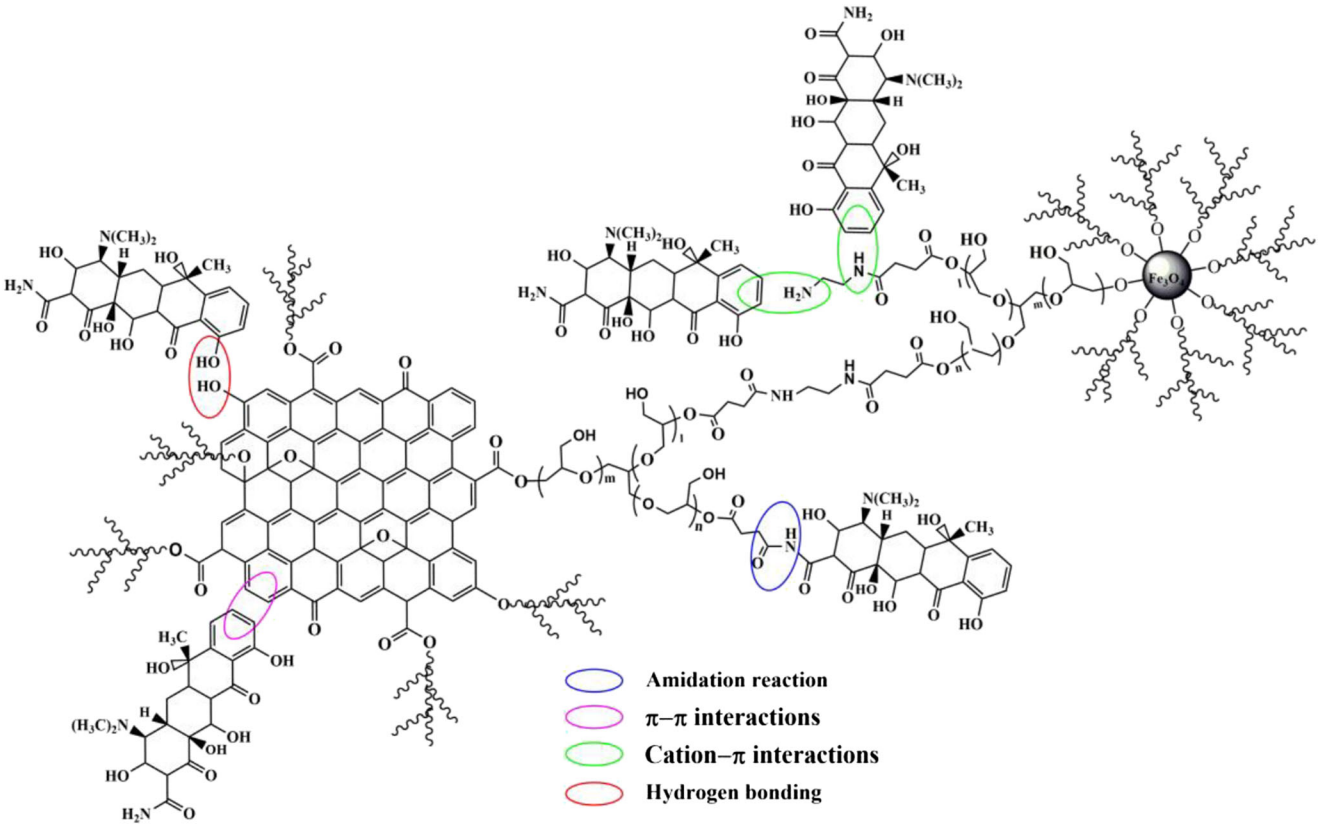

Fig. 13 The possible adsorption mechanism diagram of TC on MGON

adsorption capacity increased and reached the maximum at pH = 7.0. However, when the pH is greater than 7, the adsorption capacity decreases with the increase of pH. This adsorption trend may be due to the pH-dependent morphology of tetracycline (*pKa* values at 3.3, 7.7, and 9.7) and the surface charges of MGON (Ifebajo et al. 2018). When tetracycline is ionized in acidic (pH < 3.3) or alkaline (pH > 9.7), the removal efficiency is the lowest; when tetracycline is neutral (pH is about 7) and MGON is negatively charged in neutral solution, the removal efficiency is the highest.

Ionic strength is one of the factors affecting the adsorption capacity. The high concentration of salt in domestic and industrial wastewater may impact the elimination of organic pollutants (Xu et al. 2012). So, in this study, we investigated the effect of ionic strength on the adsorption capacity of the adsorbent when the NaCl concentration was increased from 0 to 100 mM. As shown in Fig. 11b, when the NaCl concentration is less than 60 mM, the adsorption capacity decreases with the increase of NaCl concentration, which may be attributed to the combination of Na^+ and Cl^{-1} ions with the zwitterionic drug molecules in the solution preventing effective contact of the TC with the MGON surface. Moreover, as a result of the higher positive charge of NaCl, its smaller size and its stronger ability to shield the negative charge of the MGON surface, Na^+ can be combined with vacancies produced after TC degradation. When the NaCl concentration is lower than 60 mM, the adsorption capacity decreases with the augment of NaCl concentration, indicating that the extrusion effect has dominated the salting-out effect. When the NaCl concentration is higher than 60 mM, the adsorption capacity gradually increases, which manifests that the salting out effect is enhanced with the augment of ionic strength. Hence, the increase of adsorption capacity at high ionic strength may be associated with the salting out effect and has nothing to do with electrostatic attraction (Yang et al. 2017b).

Comparison with other adsorbents

Table 4 exhibits the adsorption properties of various adsorbents for tetracycline adsorption. The TC adsorption capacity by MGON obtained from the adsorption isotherm data (Fig. 9a) is 478.43 mg/g, which is larger than the adsorption capacity of most adsorbents in the table. This suggests that MGON may be an excellent adsorbent for treating TC in domestic and industrial wastewater.

Desorption and regeneration experiments

The desorption and regeneration of adsorbents promote the reuse of pollutants, which is an important economic factor to be considered in the process. The purpose of checking the performance by simulating desorption/regeneration cycle is

to evaluate the feasibility and cost-effectiveness of large-scale application of the adsorbent. The results of desorption and regeneration are shown in Fig. 12. After five adsorption and desorption cycles, the adsorption capacity of MGON decreased while still maintaining an adsorption performance of about 67.65%. This indicates that the adsorbent has excellent regenerability and has great application potential in the removal of TC from wastewater.

Adsorption mechanism

Figure 13 depicts the possible adsorption mechanism of tetracycline on MGON. The adsorption kinetics and adsorption isotherms indicate that chemisorption dominates the adsorption process, which reveals that the possible amidation reaction between MGON and TC is one of the important factors driving adsorption. The symmetry structure of the TC molecule and the hexagonal cells of GO can produce π-π stacking interaction, which promotes the deposition of TC on MGON (Yuan et al. 2012). The electron-negative substance (hydroxyl group) in TC may combine with the hydroxyl group of the graphene oxide sheet in MGON and the oxygen-containing functional group (such as hydroxyl group and carboxyl group) on the PG layer to form a hydrogen bond to facilitate the adsorption of TC on MGON (Liu et al. 2016). The protonated amino group on the ring C_4 of the TC molecule may undergo a cationic-π interaction with the π electron on the MGON, and the easily grafted protonated amino group in MGON may also combine with π electron on TC (Li et al. 2017b). And this bonding interaction always occurs between the protonized amino group and the π electron rich structure (Ma and Dougherty 1997). Therefore, amidation, π-π stacking interactions, hydrogen bonding and cation-π interactions can be used to explain the adsorption process of TC on MGON.

Conclusion

In this study, we successfully synthesized a polyglycerol-mediated superparamagnetic graphene oxide nanocomposite called MGON, which has good dispersibility and superparamagnetism in aqueous solution. Compared with other adsorbents, MGON has an excellent adsorption capacity for tetracycline as an adsorbent with a maximum adsorption capacity of 684.93 mg/g at 298 k. The adsorption kinetics and adsorption isotherms show that the adsorption process of TC on MGON accords with pseudo-secondary kinetics and Langmuir isotherm model. The relevant parameters of adsorption thermodynamics confirm that the whole adsorption process is spontaneous and endothermic. Besides, amidation reaction, hydrogen bonding, π-π and cation-π interactions can be used to illustrate the adsorption mechanism of TC on MGON. MGON exhibited good recyclability and maintained 67.65% adsorption performance after five cycles. These results indicate that MGON is a promising environmentally treated adsorbent. In addition, the results of this experiment provide a new paradigm. Through this new method, we can develop a number of new multifunctional magnetic nanocomposites constructed by PG-mediated covalent bonds, which can be used not only for environmental treatment but also for other fields such as nanomedicine, catalysis, and energy storage.

Acknowledgments This work was supported by the Project of Innovation for Enhancing Guangdong Pharmaceutical University, Provincial Experimental Teaching Demonstration Center of Chemistry & Chemical Engineering.

References

Álvarez-Torrellas S, Rodríguez A, Ovejero G, García J (2016) Comparative adsorption performance of ibuprofen and tetracycline from aqueous solution by carbonaceous materials. Chem Eng J 283: 936–947

Badruddoza AZM, Tay ASH, Tan PY, Hidajat K, Uddin MS (2011) Carboxymethyl-β-cyclodextrin conjugated magnetic nanoparticles as nano-adsorbents for removal of copper ions: synthesis and adsorption studies. J Hazard Mater 185:1177–1186

Bu Q, Wang B, Huang J, Liu K, Deng S, Wang Y, Yu G (2016) Estimating the use of antibiotics for humans across China. Chemosphere 144: 1384–1390

Cui L, Guo X, Wei Q, Wang Y, Gao L, Yan L, Yan T, du B (2015) Removal of mercury and methylene blue from aqueous solution by xanthate functionalized magnetic graphene oxide: sorption kinetic and uptake mechanism. J Colloid Interface Sci 439:112–120

Fan L, Luo C, Li X, Lu F, Qiu H, Sun M (2012) Fabrication of novel magnetic chitosan grafted with graphene oxide to enhance adsorption properties for methyl blue. J Hazard Mater 215-216:272–279

Gadipelly C, Pérez-González A, Yadav GD, Ortiz I, Ibáñez R, Rathod VK, Marathe KV (2014) Pharmaceutical industry wastewater: review of the technologies for water treatment and reuse. Ind Eng Chem Res 53:11571–11592

Gao Y, Li Y, Zhang L, Huang H, Hu J, Shah SM, Su X (2012) Adsorption and removal of tetracycline antibiotics from aqueous solution by graphene oxide. J Colloid Interface Sci 368:540–546

Geim AK (2009) Graphene: status and prospects. Science 324:1530–1534

Gong T, Song X, Yang L, Chen T, Zhao T, Zheng T, Sun X, Gong T, Zhang Z (2019) Spontaneously formed porous structure and M1 polarization effect of Fe_3O_4 nanoparticles for enhanced antitumor therapy. Int J Pharm 559:329–340

Han Y, Cao X, Ouyang X, Sohi SP, Chen J (2016) Adsorption kinetics of magnetic biochar derived from peanut hull on removal of Cr (VI) from aqueous solution: effects of production conditions and particle size. Chemosphere 145:336–341

Han L-J, Ge F-Y, Sun G-H, Gao X-J, Zheng H-G (2019) Effective adsorption of Congo red by a MOF-based magnetic material. Dalton Trans 48:4650–4656

He F, Fan J, Ma D, Zhang L, Leung C, Chan HL (2010) The attachment of FeO nanoparticles to graphene oxide by covalent bonding. Carbon 48:3139–3144

Hu XJ, Wang JS, Liu YG, Li X, Zeng GM, Bao ZL, Zeng XX, Chen AW, Long F (2011) Adsorption of chromium (VI) by ethylenediamine-

modified cross-linked magnetic chitosan resin: isotherms, kinetics and thermodynamics. J Hazard Mater 185:306–314

Huang B, Liu Y, Li B, Liu S, Zeng G, Zeng Z, Wang X, Ning Q, Zheng B, Yang C (2017) Effect of Cu(II) ions on the enhancement of tetracycline adsorption by Fe_3O_4@SiO_2 -chitosan/graphene oxide nanocomposite. Carbohydr Polym 157:576–585

Ifebajo AO, Oladipo AA, Gazi M (2018) Efficient removal of tetracycline by CoO/$CuFe_2O_4$ derived from layered double hydroxides. Environ Chem Lett 17:487–494

Jia YC, Ke-Jing YU, Qian K, Cao HJ (2013) Study on tensile properties of carbon nanotubes/acidification graphene hybrid materials and their epoxy resin composites. Fiber Reinf Plast/compos 2:69–73

Lei Y, Chen F, Luo Y, Zhang L (2014) Three-dimensional magnetic graphene oxide foam/Fe_3O_4 nanocomposite as an efficient absorbent for Cr(VI) removal. J Mater Sci 49:4236–4245

Li Z, Chang PH, Jean JS, Jiang WT, Wang CJ (2010) Interaction between tetracycline and smectite in aqueous solution. J Colloid Interface Sci 341:311–319

Li Z, Tatsuya T, Masaaki I, Naoko K, Takahide K, Naoki K (2011) Chromatographic separation of highly soluble diamond nanoparticles prepared by polyglycerol grafting. Angew Chem Int Ed 50: 1388–1392

Li MF, Liu YG, Liu SB, Shu D, Zeng GM, Hu XJ, Tan XF, Jiang LH, Yan ZL, Cai XX (2017a) Cu(II)-influenced adsorption of ciprofloxacin from aqueous solutions by magnetic graphene oxide/nitrilotriacetic acid nanocomposite: competition and enhancement mechanisms. Chem Eng J 319:219–228

Li MF, Liu YG, Zeng GM, Liu SB, Hu XJ, Shu D, Jiang LH, Tan XF, Cai XX, Yan ZL (2017b) Tetracycline absorbed onto nitrilotriacetic acid-functionalized magnetic graphene oxide: influencing factors and uptake mechanism. J Colloid Interface Sci 485:269–279

Li MF, Liu YG, Liu SB, Zeng GM, Hu XJ, Tan XF, Jiang LH, Liu N, Wen J, Liu XH (2018) Performance of magnetic graphene oxide/diethylenetriaminepentaacetic acid nanocomposite for the tetracycline and ciprofloxacin adsorption in single and binary systems. J Colloid Interface Sci 521:150–159

Lian Y, Chen J, Zhen L, Xu W, Chen L, Ye D (2016) Degradation of phenol using Fe_3O_4-GO nanocomposite as a heterogeneous photo-Fenton catalyst. Sep Purif Technol 171:80–87

Liang J, Fang Y, Luo Y, Zeng G, Deng J, Tan X, Tang N, Li X, He X, Feng C, Ye S (2019) Magnetic nanoferromanganese oxides modified biochar derived from pine sawdust for adsorption of tetracycline hydrochloride. Environ Sci Pollut Res 26:5892–5903

Lin Y, Shen XU, Jia LI (2013) Fast and highly efficient tetracyclines removal from environmental waters by graphene oxide functionalized magnetic particles. Chem Eng J 225:679–685

Liu S, Wang H, Chai L, Li M (2016) Effects of single- and multi-organic acid ligands on adsorption of copper by Fe_3O_4/graphene oxide-supported DCTA. J Colloid Interface Sci 478:288–295

Liu R, Zhang Y, Ning Z, Xu Y (2017) A catalytic microwave process for superfast preparation of high-quality reduced graphene oxide. Angew Chem Int Ed Engl 56:15677–15682

Ma JC, Dougherty DA (1997) The cation-π interaction. Chem Rev 97: 1303–1324

Martínez JL, Coque TM, Fernando B (2015) What is a resistance gene? Ranking risk in resistomes. Nat Rev Microbiol 13:116–123

Martins AC, Pezoti O, Cazetta AL, Bedin KC, Yamazaki DAS, Bandoch GFG, Asefa T, Visentainer JV, Almeida VC (2015) Removal of tetracycline by NaOH-activated carbon produced from macadamia nut shells: kinetic and equilibrium studies. Chem Eng J 260:291–299

Mohsen A, Narjes M, Fatemeh Z (2009) Nanocapsules based on carbon nanotubes-graft-polyglycerol hybrid materials. Nanotechnology 20: 485603

Mukherjee R, Bhunia P, De S (2016) Impact of graphene oxide on removal of heavy metals using mixed matrix membrane. Chem Eng J 292:284–297

Ocampo-Pérez R, Rivera-Utrilla J, Gómez-Pacheco C, Sánchez-Polo M, López-Peñalver JJ (2012) Kinetic study of tetracycline adsorption on sludge-derived adsorbents in aqueous phase. Chem Eng J 213: 88–96

Oladipo AA, Ifebajo AO (2018) Highly efficient magnetic chicken bone biochar for removal of tetracycline and fluorescent dye from wastewater: two-stage adsorber analysis. J Environ Manag 209:9–16

Oladipo AA, Ifebajo AO, Nisar N, Ajayi OA (2017) High-performance magnetic chicken bone-based biochar for efficient removal of rhodamine-B dye and tetracycline: competitive sorption analysis. Water Sci Technol 76:373–385

Pham TA, Kumar NA, Jeong YT (2010) Covalent functionalization of graphene oxide with polyglycerol and their use as templates for anchoring magnetic nanoparticles. Synth Met 160:2028–2036

Rao CNR, Sood AK, Subrahmanyam KS, Govindaraj A (2010) Graphene: the new two-dimensional nanomaterial. Angew Chem Int Ed 48:7752–7777

Robert L et al (2013) EU-wide monitoring survey on emerging polar organic contaminants in wastewater treatment plant effluents. Water Res 47:6475–6487

Song X, Liu D, Zhang G, Frigon M, Meng X, Li K (2014) Adsorption mechanisms and the effect of oxytetracycline on activated sludge. Bioresour Technol 151:428–431

Tang WW, Zeng GM, Gong JL, Liu Y, Wang XY, Liu YY, Liu ZF, Chen L, Zhang XR, Tu DZ (2012) Simultaneous adsorption of atrazine and cu (II) from wastewater by magnetic multi-walled carbon nanotube. Chem Eng J 211-212:470–478

Wammer KH, Slattery MT, Stemig AM, Ditty JL (2011) Tetracycline photolysis in natural waters: loss of antibacterial activity. Chemosphere 85:1505–1510

Wang XM, Zhou XD, Hesketh T (2016) Massive misuse of antibiotics by university students in China: a cross-sectional survey. Lancet 388: S94–S94

Wang Y, Tang M, He S, Che G, Yu Q, Bo L (2017) Recyclable multifunctional magnetic mesoporous silica nanocomposite for ratiometric detection, rapid adsorption and efficient removal of Hg(II). ACS Sustain Chem Eng 6:1744–1752

Wang W, Yu J, Yang X, Yu B, Cai X (2019) Preparation of magnetic conjugated microporous polymers for highly efficient removal of dye from water. J Chem Technol Biotechnol 94:3333–3343

Xie G et al (2011) A facile chemical method to produce superparamagnetic grapheme oxide-Fe_3O_4 hybrid composite and its application in the removal of dyes from aqueous solution. J Mater Chem 22:1033–1039

Xie A, Dai J, Chen X, Ma P, He J, Li C, Zhou Z, Yan Y (2016) Ultrahigh adsorption of typical antibiotics onto novel hierarchical porous carbons derived from renewable lignin via halloysite nanotubes-template and in-situ activation. Chem Eng J 304:609–620

Xiong W, Zeng G, Yang Z, Zhou Y, Zhang C, Cheng M, Liu Y, Hu L, Wan J, Zhou C, Xu R, Li X (2018) Adsorption of tetracycline antibiotics from aqueous solutions on nanocomposite multi-walled carbon nanotube functionalized MIL-53(Fe) as new adsorbent. Sci Total Environ 627:235–244

Xu J, Wang L, Zhu Y (2012) Decontamination of bisphenol A from aqueous solution by graphene adsorption. Langmuir 28:8418–8425

Yang X, Wen Y, Wu A, Xu M, Amano T, Zheng L, Zhao L (2017a) Polyglycerol mediated covalent construction of magnetic mesoporous silica nanohybrid with aqueous dispersibility for drug delivery. Mater Sci Eng C Mater Biol Appl 80:517–525

Yang Y, Hu X, Zhao Y, Cui L, Huang Z, Long J, Xu J, Deng J, Wu C, Liao W (2017b) Decontamination of tetracycline by thiourea-dioxide–reduced magnetic graphene oxide: effects of pH, ionic strength, and humic acid concentration. J Colloid Interface Sci 495:68–77

Yang X, Li A, Wang W, Zhang C, Wang J, Yu B, Cai X (2018a) Synthesis of polyglycerol mediated covalent construction of a core-satellite superparamagnetic mesoporous carbon nanocomposite: application on dye adsorption. J Chem Technol Biotechnol 93:2635–2643

Yang X, Zhao L, Zheng L, Xu M, Cai X (2018b) Polyglycerol grafting and RGD peptide conjugation on MnO nanoclusters for enhanced colloidal stability, selective cellular uptake and cytotoxicity. Colloids Surf B 163:167–174

Yang X, Zhang C, Li A, Wang J, Cai X (2019) Red fluorescent ZnO nanoparticle grafted with polyglycerol and conjugated RGD peptide as drug delivery vehicles for efficient target cancer therapy. Mater Sci Eng C Mater Biol Appl 95:104–113

Yao Y, Miao S, Liu SZ, Li P, Sun H, Wang S (2012) Synthesis, characterization, and adsorption properties of magnetic Fe_3O_4@graphene nanocomposite. Chem Eng J 184:326–332

Yu B, Bai Y, Ming Z, Yang H, Chen L, Hu X, Feng S, Yang ST (2017) Adsorption behaviors of tetracycline on magnetic graphene oxide sponge. Mater Chem Phys 198:283–290

Yuan G, Yan L, Liang Z, Hui H, Junjie H, Syed Mazhar S, Xingguang S (2012) Adsorption and removal of tetracycline antibiotics from aqueous solution by graphene oxide. J Colloid Interface Sci 368: 540–546

Zhang D, Yin J, Zhao J, Zhu H, Wang C (2015) Adsorption and removal of tetracycline from water by petroleum coke-derived highly porous activated carbon. J Environ Chem Eng 3:1504–1512

Zhang J, Khan MA, Xia M, Abdo AM, Lei W, Liao C, Wang F (2019a) Facile hydrothermal synthesis of magnetic adsorbent $CoFe_2O_4$/MMT to eliminate antibiotics in aqueous phase: tetracycline and ciprofloxacin. Environ Sci Pollut Res Int 26:215–226

Zhang X, Lin X, He Y, Chen Y, Luo X, Shang R (2019b) Study on adsorption of tetracycline by cu-immobilized alginate adsorbent from water environment. Int J Biol Macromol 124:418–428

Zhao L, Chano T, Morikawa S, Saito Y, Shiino A, Shimizu S, Maeda T, Irie T, Aonuma S, Okabe H, Kimura T, Inubushi T, Komatsu N (2012) Hyperbranched polyglycerol-grafted superparamagnetic iron oxide nanoparticles: synthesis, characterization, functionalization, size separation, magnetic properties, and biological applications. Adv Funct Mater 22:5107–5117